Dielectric capacity, liquid water content, and pore structure of thawing-freezing materials

Antonin Fabbri, Teddy Fen-Chong*, Olivier Coussy

Institut Navier, LMSGC 2 allée Kepler - 77420 Champs-sur-Marne, France

Abstract

A capacitive sensor-based experimental approach is worked out to study the ice / water phase change in cohesive porous media subject to freezing and thawing. This technique relies upon the dielectric properties of liquid water, ice, air, and mineral substrate in the radio-frequency range. A semi-empirical method based upon the Lichtenecker model and combining drying and freezing tests, provides an accurate estimation of the liquid water content versus the temperature in freezing cement pastes. This estimation is further analysed with the help of thermoporometry concepts in order to characterize the pore size distribution and the specific surface area. The results range in the same order of magnitude as those assessed from gravimetric sorption/desorption isotherms.

Keywords: Porous media, freezing, thawing, dielectric, capacitive method, supercooling, liquid water amount, pore size distribution, specific surface, sorption / desorption isotherm, cement.

*Corresponding author: fenchong@lcpc.fr, tél: +33140435451, fax: +33140435450

1 Introduction

Damage induced by frost action upon concrete structures is a source of main concern in cold climates [Pigeon, 1984, Dash et al., 1995]. Contrary to an obvious possible explanation, damage in concrete cannot originate from only the expansion undergone by liquid water when transforming to ice: sample expansion is still observed in cement pastes saturated with benzene, whose density increases with solidification [Beaudoin and MacInnis, 1974]. Actually, confined liquid water within a porous material submitted to frost action does not simultaneously freeze at the same temperature. This is commonly attributed to the interaction between water and pore surfaces, water impurity, or supercooling [Scherer, 1993, Dash et al., 1995]. As a consequence, an initially water-saturated porous material remains filled by both ice and liquid water down to at least $-80\ ^0$C [Jehng et al., 1996]. Nowadays, the mechanical response of a porous material is credited to result from the combination of the liquid-solid expansion, the transport of unfrozen liquid water through the porous network, and the presence of air voids [Wang et al., 1996]. A poromechanics-based approach has been recently worked out to understand and quantify the phenomena both at the pore scale [Coussy and Fen-Chong, 2005] and at the material scale [Coussy, 2005]. Whatever the approach carried out, the freezing / thawing curve, that is the saturation degree of unfrozen water versus temperature, turns out to be the key curve governing the mechanical behaviour of porous materials upon frost action. That is why the liquid water content as a function of the temperature has been investigated in partially frozen porous media by nuclear magnetic resonance [Watanabe and Mizogucchi, 2002], differential scanning

calorimetry [Kozlowski, 2003a, Kozlowski, 2003b], acoustic approach [Thimus et al., 1991], or time domain reflectometry [Spaans and Baker, 1995], on loosely bonded porous media like silty, clayey soils, or silica glass powders.

Freezing of cement based materials is usually studied with low temperature calorimetry [Bager and Sellevold, 1986]. However, temperature calorimetry applies only to millimetric specimens which in addition are often crushed. Tests on non-crushed heterogeneous materials, like mortar and concrete exhibiting centimetric aggregates, remain difficult to perform using this technique. For such materials requiring larger samples, the dielectric method [Tran and Dupas, 1988] is more appropriate, while being less expensive. This article explores a spectroscopic-like dielectric capacitive method and analyses the results it provides on the ice / liquid water transform in cohesive porous materials such as cement pastes.

2 Dielectric capacitive method

2.1 Principle and experimental apparatus

The dielectric relaxation time τ of liquid water is much smaller than the one related to ice crystal (resp. 10^{-10} s and 10^{-5} s). As a consequence, for an electrical field lying in the radio-frequency range 10 - 100 MHz, the dielectric constant of liquid water is still equal to its static value, that is between 80 and 100, whereas the permittivity of ice is equal to its optical value which is close to 3. Figure 1 shows the real dielectric constants ε of liquid water and ice against the frequency f of the exciting electrical field for various

values of the temperature θ (in Celsius degree). These curves assume that the dielectric behaviour of ice and liquid water are well-described by the single relaxation time-based Debye model [Cole and Cole, 1941, Ellison et al., 1996, Kaatze, 1997]:

$$\varepsilon(f,\theta) = \Re e\left(\varepsilon_{\to\infty} + \frac{\varepsilon_{\to 0}(\theta) - \varepsilon_{\to\infty}}{1 + j\,2\pi f\,\tau}\right) \tag{1}$$

where $\varepsilon_{\to\infty}$ is the limit permittivity for f going to infinity, while $\varepsilon_{\to 0}$ the static permittivity. In addition to the high ice / liquid water dielectric constant contrast, experimental tests on air and dry mineral samples also indicate that the real dielectric constants of the latter are close to the optical dielectric constant of ice; 1 for air, and between 3 and 10 for mineral materials. Hence, any change in the liquid water content, due to solidification / melting or condensation / evaporation, within a porous medium will significantly affect the overall material dielectric constant. Accordingly, the measurement of the latter leads to an indirect assessment of the current liquid water content.

The capacitive method consists in measuring the dielectric constant through the electric capacitance C of a sample submitted to an electrical field in the above mentioned radio-frequency range. Actually the sample dielectric constant ε can be then evaluated according to:

$$C = \varepsilon C_0 = \varepsilon \frac{\varepsilon_0 S}{e} \tag{2}$$

with C_0 the empty capacitance, $\varepsilon_0 = \frac{1}{36\pi} 10^{-9}$ F/m the vacuum permittivity, while S and e are the electrode surface and the distance between the two plane electrodes. The experimental set-up, its calibration, and its use to study the drying of porous stones and fused glass beads have been already described in [Fen-Chong et al., 2004], while an account of a

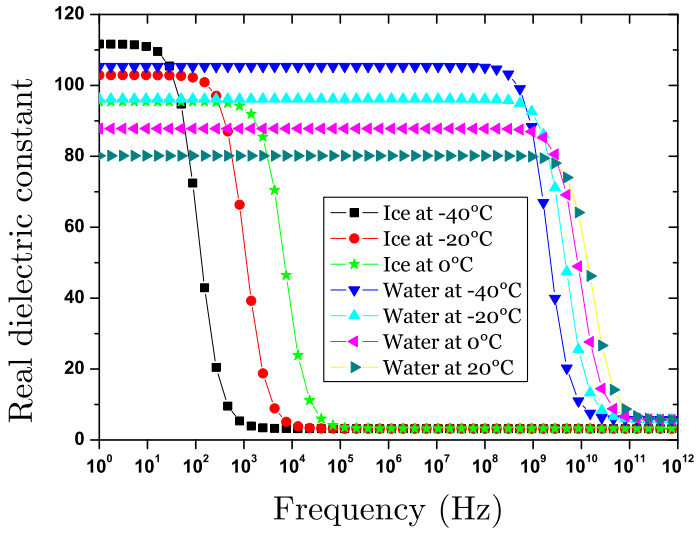

Figure 1: Frequency dispersion of water and ice real dielectric constants at different temperatures.

preliminary work on freezing and thawing study is presented in [Fen-Chong et al., 2005]. As sketched out in figure 2, the sample is inserted between two plane and circular stainless steel electrodes. A 30 MHz - 50 MHz oscillator in parallel with the sample achieves to form an oscillating circuit, whose experimental apparatus measures the reduced frequency, f_{red} that is the resonant frequency f divided by 5632. The resonant frequency depends on the overall capacitance of the sample, the electrical wires and the oscillator. Due to the impossibility of accurately separating the contribution of each component, the relation between the reduced frequency and the capacitance of the sample itself was obtained with the help of different liquids of well-known dielectric constant. The capacitance of samples made up of glass containers filled by these fluids was then calculated from equation (2) and plotted against the corresponding measured value f_{red}. As presented in figure 3, the $f_{red} - C$ relation is linear and agrees with measurements previously performed by [Tran and Dupas, 1988, Djaballah-Masmoundi, 1998] by means of a similar capacitive apparatus. By measuring the changes in the sample capacity C and by using (2), the experimental apparatus finally allows to determine the changes in the dielectric constant ε versus relative humidity or temperature.

2.2 Liquid saturation degree and dielectric constants

The next step in the capacitive method is to determine the relation existing between the sample dielectric constant ε which is actually measured, and the physical quantity of interest, here the liquid saturation degree S_w which is the ratio between the volume occupied by liquid water and the overall porous volume. To determine the $\varepsilon - S_w$ relation,

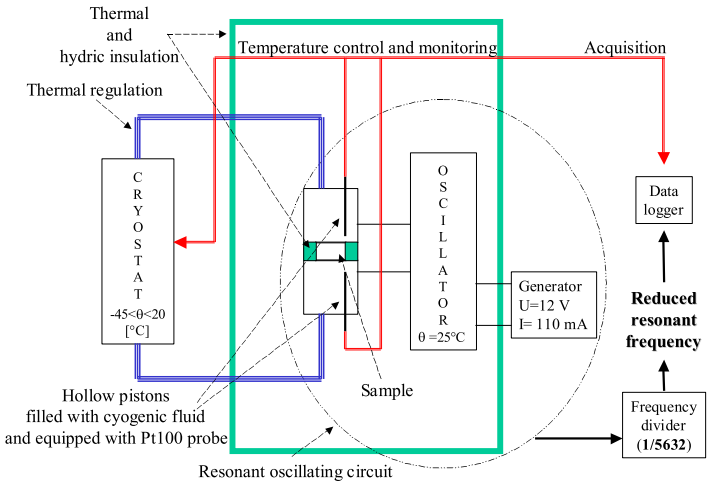

Figure 2: Schematic diagram of the capacitive sensor-based apparatus. The oscillator was implementing a frequency divider in order to reach a low frequency range (in the order of several kHz) before outputting the resonant frequency to the data logger device. Galden PFPE HT200 from Solvay Solexis company is used as cryogenic fluid for its low static dielectric constant (about 2 at 20 ^{0}C).

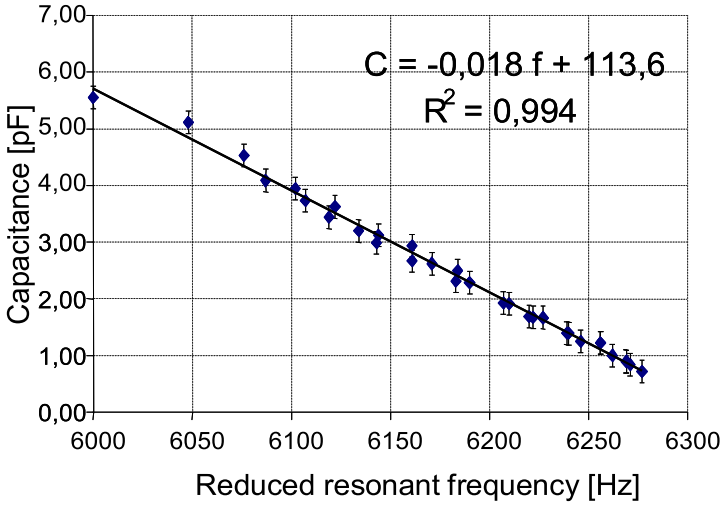

Figure 3: Sample-electrode capacitance versus measured reduced resonant frequency.

after reviewing some classical multi-scale schemes [Zakri et al., 1998, Mironov et al., 2003, Zhang et al., 2003, Bitteli et al., 2004, Fen-Chong et al., 2004]), the Lichtenecker model was eventually chosen since it is widely recognized to well apply to dielectric heterogeneous materials. This model is based upon an effective medium approach in which the self-consistent scheme is adopted and where a beta function accounts for the probability density of the ellipsoidal inclusion shape. For n constituents, whose related volume ratio is $\phi_{k=1,n}$, the Lichtenecker model finally gives (the proof is summarized in [Zakri et al., 1998]):

$$\varepsilon = \left(\sum_{k=1}^{k=n} \phi_k \, \varepsilon_k^{\alpha} \right)^{1/\alpha} \quad ; \; -1 \leq \alpha < 0; \quad 0 < \alpha \leq 1 \tag{3}$$

When $\alpha = 1$ the pores (void inclusions) are parallel to the external field, while for $\alpha = -1$ they are perpendicular to the external field. The previous expression does not apply

for $\alpha = 0$ for which no particular shape nor orientation is privileged with regard to the direction of the external field. For such a completely disordered medium the Lichtenecker model provides ε in the form:

$$\varepsilon = \prod_{k=1}^{k=n} \varepsilon_k^{\phi_k} \tag{4}$$

For the case at hand the pore volume filled both by liquid water, with dielectric constant ε_w, and by a non wetting component, say here ice crystal or air, with dielectric constant ε_{nw}, is considered as an effective medium. Its dielectric constant ε_p is then given by (3) where we let $n = 2,\ k \equiv w$ or nw, while $\phi_w = S_w$ and $\phi_{nw} = (1 - S_w)$:

$$\varepsilon_p = \left(S_w \varepsilon_w^\alpha + (1 - S_w)\, \varepsilon_{nw}^\alpha\right)^{1/\alpha} \tag{5}$$

In a first approach no particular pore shape nor orientation is assumed to be privileged. Letting ε_m be the dielectric constant of the solid mineral matrix, the overall dielectric constant ε is then provided by setting $n = 2,\ k \equiv p$ or m, $\phi_m = 1 - \phi$ and $\phi_p = \phi$ (where ϕ is the overall porosity) in (4), and by substituting (5) for ε_p:

$$\varepsilon = \varepsilon_m^{1-\phi} \left(S_w \varepsilon_w^\alpha + (1 - S_w)\, \varepsilon_{nw}^\alpha\right)^{\phi/\alpha} \tag{6}$$

At this stage the assumption of a disordered pore structure still needs to be confirmed, and parameter α experimentally determined.

3 Tested materials and related properties

3.1 Materials

Cement paste samples, with water-cement ratio 0.4 and 0.5, were prepared with a 5-liter mortar mixer, and cast in 100 mm high cylindrical moulds with a 40 mm diameter. Ordinary Portland Cement CEM I CPA 52.5 N CP2 and distilled water were used. One day after casting, specimens were removed from their mould and stored in moist condition (relative humidity $rh = 95\% \pm 5\%$) during 6 months. They were further cut in 15 mm thick slices and remained in water before tested. All specimens were characterized by mercury intrusion porosimetry (MIP) and gravimetric sorption/desorption isotherm (SD) tests. The former is used in order to evaluate porosity (tables 1 and 2) and specific surface area (table 6). The latter is a home-made apparatus described in [Raoof and Guilbaud, 1995]. It is used in order to evaluate specific surface area (table 6) and pore radii distribution (figures 10 and 11). Specimens were saturated with degassed distilled water at 3 kPa air pressure and tested. Before saturation, some specimens (index d) were dried in an oven at 70 ^{0}C and one specimen (P4-3) was dried during 6 months in a 11%-rh controlled recipient. Finally, solid matrix dielectric constants are evaluated from the dielectric constant ε provided directly by the capacitive sensor apparatus (CS) and by using the method soon to be described. Cement paste characteristics are reported in table 1.

Our main experimental apparatus goal is to evaluate the ice content forming in a cementitious material. However, the dielectric properties of the in-pore water of cement-based materials are not well known, nor easy to evaluate (high ionic strength, adsorption

	e[cm]	D[cm]	ϕ ($\pm$0.01)	ϕ_{MIP}	$\varepsilon_m(\pm 0.2)$
P4-1d	1.33	3.9	0.296	0.178	11.5
P4-2	1.36	3.85	0.308	0.170	8.34
P4-3	1.55	3.9	0.260	0.168	11.8
P5-1d	1.42	3.94	0.361	0.208	10.3
P5-2	1.49	3.95	0.352	0.232	13.2

Table 1: Cement paste characteristics: ϕ is the water porosity (i.e. evaluated from the sample mass difference between dried and saturated states), ϕ_{MIP} the porosity estimated by MIP, ε_m the solid matrix dielectric constant at 20 ^{0}C.

phenomena). Accordingly, the device calibration and the same characterization tests were also made with two different model porous media like fused glass beads and Caen stones, the main characteristics of which are reported in table 2.

	e[cm]	D[cm]	ϕ	ϕ_{MIP}	$\varepsilon_m(\pm 0.2)$
Caen Stone	1.01	3.96	0.39$\pm$0.05	0.39$\pm$0.05	7.6
Fused glass beads	1.00	5.01	0.10.$\pm$0.01	0.09$\pm$0.01	5.9

Table 2: Model porous media characteristics: ϕ is the water porosity, ϕ_{MIP} the porosity estimated by MIP, ε_m the solid matrix dielectric constant at 20 ^{0}C.

3.2 Dielectric constants

Since the in-pore solution contains ions and impurities, its dielectric constant ε_w is not equal to the one of pure water. To obtain a solution close to the in-pore one, the tested sample is inserted in a small recipient containing initially distilled water. When the pH of the outer solution in the recipient becomes constant, chemical equilibrium is reached. Hence the in-pore and the recipient solutions can be considered as similar. Then ε_w are evaluated from the recipient solutions dielectric constant measurement. The corresponding values related to the tested materials are reported in table 3. The high values of ε_w found for cement paste can be explained by the ion hydration which produces some polar species resulting in dielectric amplification [Barthel et al., 1992] in the used frequency range.

	Caen Stone	fused glass beads	P5-1d
ε_w (20^0C)	75 $\pm$5	80 $\pm$5	250 $\pm$25

Table 3: In-pore water dielectric constant.

The mineral substrate dielectric constant ε_m was obtained by saturating the porous material with fluids exhibiting different values for the dielectric constant ε_f; air ($\varepsilon_f = \varepsilon_a = 1$), hexane ($\varepsilon_f = 1.9$), ethanol ($\varepsilon_f = 25$), and finally water ($\varepsilon_f = \varepsilon_w$). The actual overall dielectric constant ε related to each sample so saturated was then measured, providing an experimental curve $\varepsilon = f(\varepsilon_f)$. Estimation of ε_m was carried out by looking for the dielectric constant of an in-pore fictitious fluid such that the sample is dielectrically ho-

mogeneous, turning out to solve the equation $\varepsilon_m = f(\varepsilon_m)$. The values of ε_m so obtained are reported in table 1 for the cement pastes, and table 2 for the model porous media.

Knowing the dielectric constant of each phase, the relevancy of relation (6) giving the overall dielectric constant as a function of the liquid saturation can be tested, and parameter α determined. To this aim the dielectric constant ε of saturated samples were measured and plotted against the dielectric constant ε_f of the saturating fluid. The experimental curve from two-phase samples composed of the matrix and a fully saturating fluid is shown in figure 4. It is accurately accounted for by substituting ε_f to ε_w and letting $S_w = 1$ in (6). This eventually supports the relevancy of a disordered pore structure. Parameter α was then determined from a drying test. At successive stages of drying the overall dielectric constant ε is measured and plotted against the liquid saturation degree S_w obtained by comparing the current sample weight to the initial one. Figure 5 shows a linear relation between ε and S_w, which is well accounted for by letting $\alpha = \phi$ in (6). Accordingly, the overall dielectric constant $\varepsilon_{w,nw}$ of the porous materials here analyzed, saturated by liquid water (index w) and a complementary non wetting component (index nw), is written:

$$\varepsilon_{w,nw} = \varepsilon_m^{1-\phi} \left(S_w \varepsilon_w^{\phi} + (1 - S_w) \varepsilon_{nw}^{\phi} \right) \tag{7}$$

However (7) was obtained at $\theta = 20\ ^0$C at which the matrix and pore water dielectric constants, ε_m and ε_w, are both known. Actually, the in-situ dielectric constant of in-pore liquid water varies with ionic strength [Barthel et al., 1992, Kaatze, 1997] and adsorption [Mercury et al., 2001], which in turn depend on temperature and saturation. Fur-

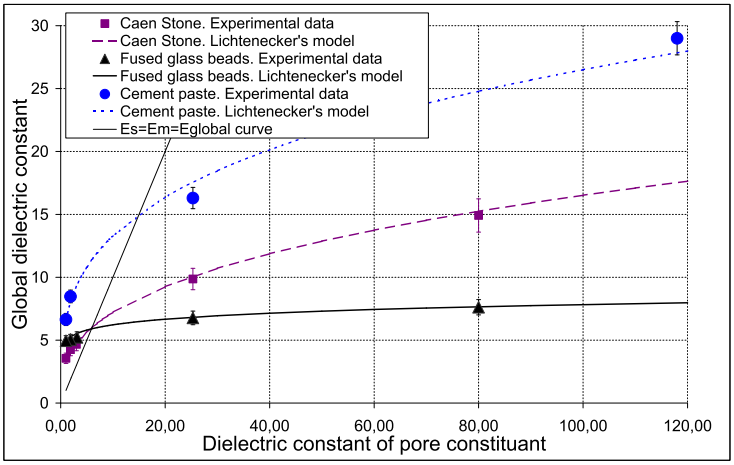

Figure 4: Comparison between measured and calculated dielectric constants of a fully saturated porous medium. The calculation is made using the two-phase Lichtenecker model with (4) or (6) in which $\varepsilon_w = \varepsilon_f$ and $S_w = 1$.

thermore the change of the dielectric constant of non-evaporable water with temperature will significantly affect the matrix dielectric constant. As a consequence a further relation is needed between $\varepsilon_{w,nw}, S_w$ and θ.

4 Semi-empirical approach for liquid water content in frozen cement paste

The in-pore water of cement paste in the range of low liquid saturation degrees $S_w < 0.5$ was experimentally found not to freeze down to -45 ^{0}C. This was previously observed

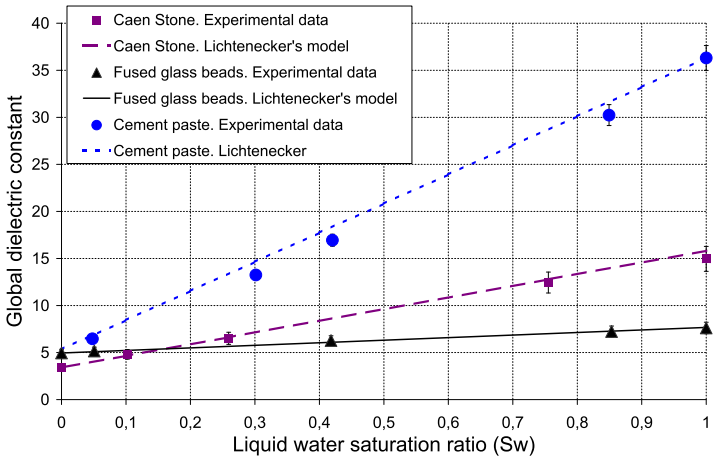

Figure 5: Comparison between measured and calculated dielectric constants of a non-saturated porous medium. The calculation is made using the three-phase Lichtenecker model with $\alpha = \phi$ in (6), thus leading to (7).

by [Kaufmann, 1999]. Assuming that no pore water evaporation takes place during cooling/heating cycle on such low saturated samples in the temperature range [0 ^{0}C; -45 ^{0}C], it becomes possible to experimentally determine the relation between the (initial) liquid water degree saturation, the temperature, and the sample dielectric constant $\varepsilon_{w,a}$, where index a refers to air. For partially frozen cement pastes, this relation can be then combined with (7) to account for the difference between the dielectric constants of air and ice crystal. This semi-empirical approach is presented below.

4.1 Dielectric constants of unsaturated cement pastes

The changes in the dielectric constant $\varepsilon_{w,a}$ with respect to temperature were first determined at liquid saturation degree S_w held constant. Samples with different liquid saturation degrees S_w were prepared by conserving initially dried specimens in an oven at 70 ^{0}C during 6 months, within atmospheres at various controlled humidity rh =12%, 33%, 44%, 85%, and 100% by using salt solutions [Raoof, 1998]. This procedure provided samples with liquid water saturation degrees S_w =0.12, 0.17, 0.18, 0.49 and 1 respectively. The sample dielectric constant $\varepsilon_{w,a}$ was then determined from 20 ^{0}C to -5 ^{0}C for $S_w = 100\%$, and from 20 ^{0}C to -40 ^{0}C for S_w =0.12, 0.17, 0.18, 0.49. It must be again stressed out that these temperature ranges were allowed since primary freezing occurs only at -5 ^{0}C for saturated cement pastes, and no freezing is observed for unsaturated cement pastes with $S_w < 0.5$ before -45 ^{0}C. Whatever the porous material tested here, the relation between the dielectric constant $\varepsilon_{w,a}$ and the temperature was found to be linear (see figure 6A for cement paste P5-1d), so that the corresponding slope $a(S_w)$ is a function of

liquid saturation only. Furthermore, as reported in figure 6B, $a(S_w)$ curve was found to be a line. We finally write:

$$\frac{\partial \varepsilon_{w,a}}{\partial \theta} \mid_{S_w} = a \times S_w + b \tag{8}$$

with $a \simeq 0.225\ ^0\mathrm{C}^{-1}$ and $b \simeq 0.002\ ^0\mathrm{C}^{-1}$.

Irrespective to the previous experiments the changes in the dielectric constant $\varepsilon_{w,a}$ with respect to liquid saturation S_w were then determined at temperature held constant. By varying the relative humidity rh, drying tests were performed at different temperatures (6 drying tests from $20\ ^0\mathrm{C}$ to $-5\ ^0\mathrm{C}$). As found in [Fen-Chong et al., 2004] and reported in figure 7A for cement paste P5-1d, all tests provide a linear relation between the dielectric constant $\varepsilon_{w,a}$ and the liquid saturation degree S_w. As a consequence, the corresponding slope b is a function of temperature θ only. Furthermore, as reported in figure 7B, $b\,(\theta)$ is found to be a line. We finally write:

$$\frac{\partial \varepsilon_{w,a}}{\partial S_w} \mid_{\theta} = b(\theta) = a' \times \theta + c \tag{9}$$

with $a' \simeq 0.227\ ^0\mathrm{C}^{-1}$ and $c \simeq 20.158$.

The Maxwell symmetry-like relation $\frac{\partial^2 \varepsilon_{w,a}}{\partial \theta \partial S_w} = \frac{\partial^2 \varepsilon_{w,a}}{\partial S_w \partial \theta} \Longleftrightarrow a \simeq a' = 0.23$ so obtained confirms the existence of a material relation linking $\varepsilon_{w,nw}$, S_w and θ only. This was also observed for stone and fused bead glass samples. For the tested porous materials, we can eventually write:

$$\varepsilon_{w,a} = a \times S_w \times \theta + b \times \theta + c \times S_w + d \tag{10}$$

where coefficients a, b, c, d are specific to the tested porous material. Their determination requires two tests only: cooling of a fully saturated sample ($S_w = 1$) down to the primary

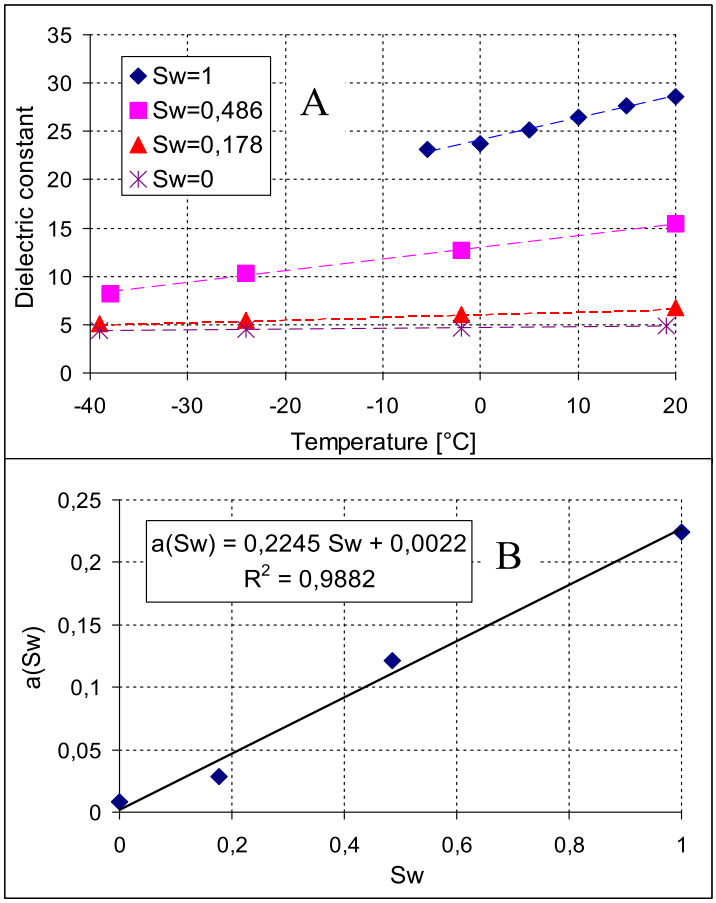

Figure 6: Evolution of the apparent dielectric constant and its derivation with temperature at a fixed saturation ratio for cement paste P5-1d.

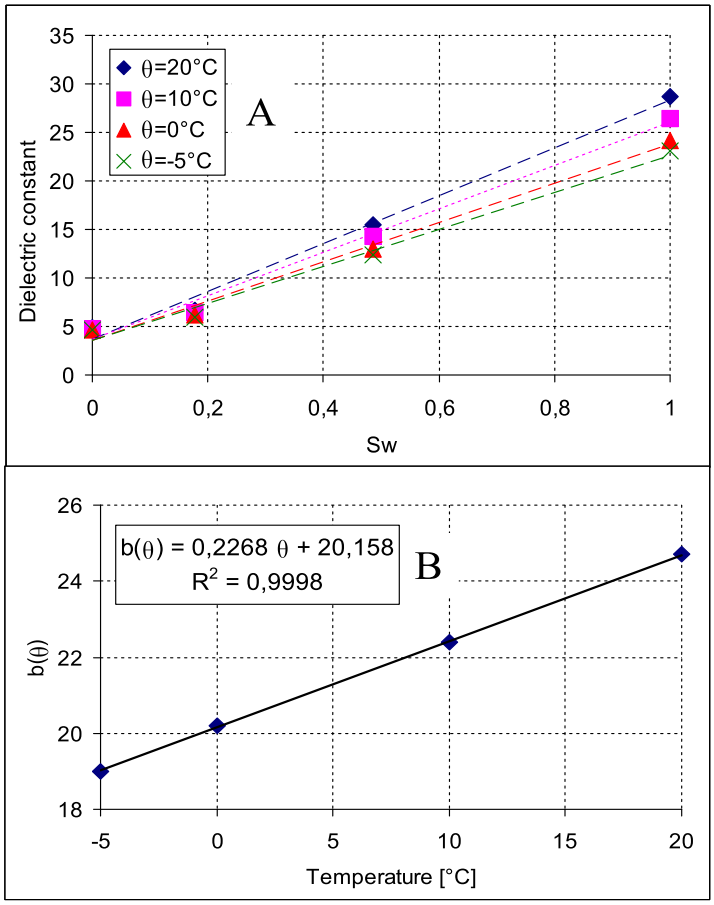

Figure 7: Evolution of the apparent dielectric constant and its derivation with saturation at a fixed temperature for cement paste P5-1d.

freezing, and a cooling test of a dried sample ($S_w = 0$) down to -45 ^{0}C.

4.2 From in-pore air/water to ice/water mixtures

Using (7), we now write:

$$\varepsilon_{w,i} = \varepsilon_{w,a} + \varepsilon_m^{1-\phi}(1 - S_w)(\varepsilon_i^{\phi} - \varepsilon_a^{\phi}) \tag{11}$$

with index i refering to ice. Further, (7) and (10), where we let $S_w = 0$ and $\varepsilon_{nw} = \varepsilon_a = 1$, combine to:

$$\varepsilon_m^{1-\phi} = \varepsilon_{w,a}(S_w = 0, \theta) = b \times \theta + d \tag{12}$$

Substitution of (10) and (12) into (11) finally provides:

$$\varepsilon_{w,i} = A \times S_w \times \theta + B \times \theta + C \times S_w + D \tag{13}$$

where:

$$A = a - b(\varepsilon_i^{\phi} - 1); \quad B = b\varepsilon_i^{\phi}\beta; \quad C = c - d(\varepsilon_i^{\phi} - 1); \quad D = d\varepsilon_i^{\phi} \tag{14}$$

Once the changes in $\varepsilon_{w,i}$ with respect to experimentally determined temperature, semi-empirical relation (13) gives the means to determine the thermodynamic state function linking S_w to θ.

5 Results: Freezing and thawing curves

Figures 8 and 9 show the estimated liquid water saturation ratio variation with temperature during the cooling and heating stages of the P4 and P5 cement paste samples.

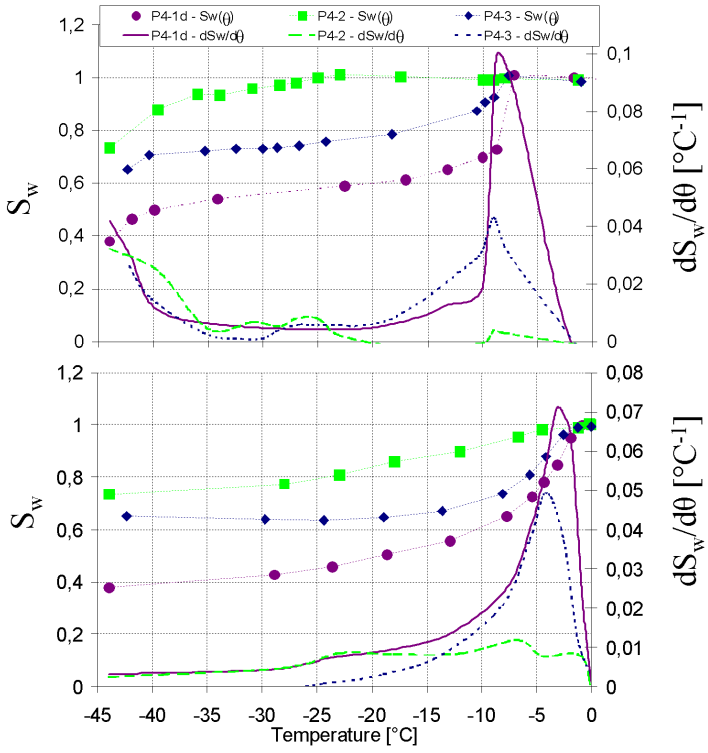

Figure 8: Freezing (upper graph) and thawing (lower graph) of $W/C = 0.4$ cement paste submitted to different curing conditions.

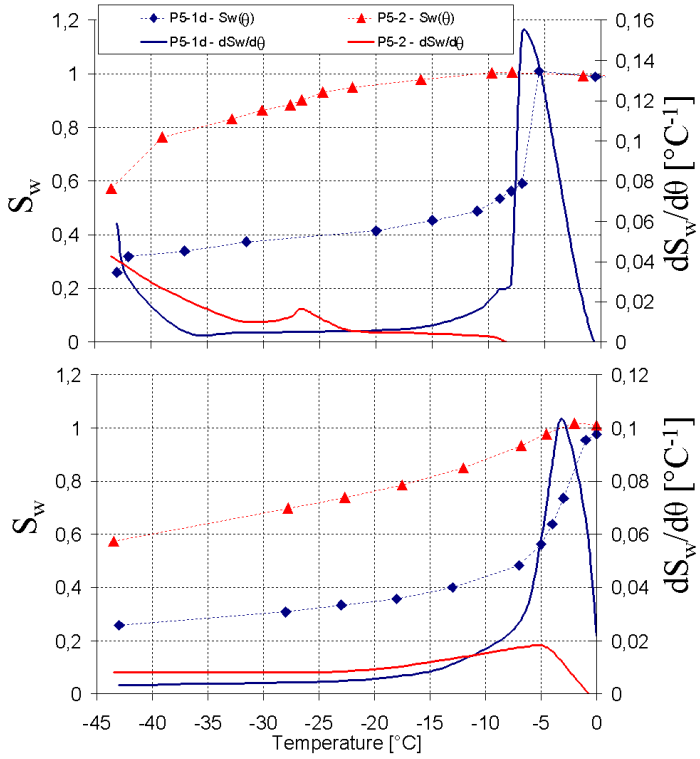

Figure 9: Freezing (upper graph) and thawing (lower graph) of $W/C = 0.5$ cement paste submitted to different curing conditions.

Saturation varies almost linearly with temperature, except in the range of three particular temperatures on cooling, around -8 ^{0}C, -25 ^{0}C and -43 ^{0}C, and one, around -3 ^{0}C on heating, where the slope changes significantly. The linear saturation variation is related to the progressive freezing (resp. thawing) of the water (resp. ice) contained in the connected pores which are sufficiently big (resp. small) to freeze (resp. thaw). The saturation slope change is due to an important water / ice phase change. The presence of these peaks is in good agreement with the data given in the literature (see table 4).

Ref.	P4-1d	P4-2	P4-3	P5-1d	P5-2	Ref. A		Ref. B	
W/C	0.4			0.5		0.4	0.5	0.4	0.4
Drying	70°C	$rh95\%$	$rh11\%$	70°C	$rh95\%$	97°C	none	none	$rh11\%$
θ_1 [°C]	-8	*	-8	-5	-10	-10	-5	*	-10
w_1 [%]	4.5	*	1.1	8	0.5	?	?	*	2
θ_2 [°C]	*	-28	-28	*	-27	*	-25	-25	-25
w_2 [%]	*	0.4	3.5	*	2	*	?	0.5	3
θ_3 [°C]	-44	-45	-43	-42	-40	-40	-43	-40	-42
w_3 [%]	10	3.5	5	14	8.5	12	7	2.5	4.5

Table 4: Results obtained for capacitive sensor based apparatus (this study) and low temperature calorimetry from [Sellevold and Bager, 1980] (ref. A) and [Bager and Sellevold, 1986] (ref. B): θ_x and w_x stand for the x^{th} freezing peak temperature (in Celsius degree) and freezable water content (in %).

For specimens oven-dried before testing (P4-1d and P5-1d), an important freezing peak is observed around -8 ^{0}C and a minor second one around -43 ^{0}C. The lack of the θ_2 peak in our work is also reported on the same kind of paste by [Lindmark, 1997, Kaufmann, 1999, Béjaoui et al., 2002]. For specimen dried at $rh = 11\%$ (P4-3), three peaks are detected at -8 ^{0}C, -28 ^{0}C, and -43 ^{0}C. On virgin specimens (P4-2 and P5-2), the first freezing peak is almost absent while the θ_2 and θ_3 peaks are pronounced. Similar results were obtained by [Sellevold and Bager, 1980]. In summary, it appears that drying the sample increases the first freezing θ_1 peak and reduces the two others (θ_2 and θ_3).

Actually, from studies made with low temperature calorimetry [Béjaoui et al., 2002] and nuclear magnetic resonance [Jehng et al., 1996], a maximum of three distinct sort of pores, associated with the three freezing peaks, could be observed in a freezing test: large capillaries ($r_c \simeq 100$ nm, $\theta = \theta_1$), small capillaries ($r_c \simeq 10$ nm, $\theta = \theta_2$) and open gel pores ($r_c \simeq 1$ nm, $\theta = \theta_3$). Thus, the reduction of second and third freezing peaks can be explained by microcraking-like damage produced by oven-drying that reduces the proportion of open gel pores and raises the proportion of small and large capillary ones. This explanation is relevant with the simultaneous first freezing peak increase observed for P4-1d and P5-1d.

Our data are compared with low temperature calorimetry ones on the same kind of specimen. As the liquid water saturation ratio depends on the dry sample mass m_{dry} (recall that $S_w = V_w/V_{pores} = (m - m_{dry})/(m_{sat} - m_{dry})$; m is the sample mass, m_{sat} is the saturated sample mass) which varies noticeably with the drying method used [Gallé, 2001],

comparisons were made on ice contents values ($w_i = m_i/m_{ssd}$, with m_i the mass of ice formed, and m_{ssd} the sample saturated dried-surfaces mass). Results are reported in table 5. Measured relative differences Δ_i are always smaller than 20% in the exception of W/C=0.4 virgin pastes second peak and 11%-rh cured pastes first peak. These high Δ_i values can be explained by the common lack of reproducibility between two cement paste materials which are not of the same batch. Moreover, only a small quantity of ice is formed in this kind of material, thus small absolute differences result in high Δ_i.

Hence, results found with the capacitive sensor based apparatus are in good agreement with literature data from [Sellevold and Bager, 1980] and [Bager and Sellevold, 1986].

W/C	0.4	0.4	0.4	0.5
Drying	oven-dried	rh 11%	virgin	virgin
Δ_1 (%)	?	50	*	?
Δ_2 (%)	?	14.3	20	?
Δ_3 (%)	12	10	28	18

Table 5: Comparison between capacitive sensor based apparatus and low temperature calorimetry results. Δ_x stand for the x^{th} relative difference (in %) between freezable water content literature data from table 4 and values obtained in this study for similar W/C ratio and curing method.

6 Porous network characterization

6.1 Relation between freezing temperature and porous distribution

The thermodynamic equilibrium between water in liquid form (index w) and its ice crystal (index i) requires the equality of their specific chemical potentials, reading:

$$\mu_i = \mu_w \tag{15}$$

The natural arguments of the chemical potential μ_J per mass unit of phase $J = w$ or i, are the absolute temperature T ($T\,[\mathrm{K}] = \theta\left[\,^0\mathrm{C}\right] + 237.15$) and the current pressure p_J. Hereafter the atmospheric pressure (conveniently set equal to zero in all that follows) is adopted as the common reference pressure and the corresponding freezing point T_0 as the reference temperature. From the differentiation of (15), standard thermodynamics furnishes:

$$\frac{1}{\rho_i}\mathrm{d}p_i - s_i\mathrm{d}T = \frac{1}{\rho_w}\mathrm{d}p_w - s_w\mathrm{d}T \tag{16}$$

where ρ_J is the mass density which will be taken to be constant and associated with the reference state ($\rho_i \simeq 0.9167$ g/cm^3 and $\rho_w \simeq 0.9998$ g/cm^3 [Petrenko and Whitworth, 1999]), and s_J are the entropy per mass unit of phase J.

Since the strain latent heat and the variation of heat capacity with temperature are negligible, the specific entropy is written as:

$$s_J = s_J^0 + c_{p,J}\ \ln\frac{T}{T_0} \tag{17}$$

with s_J^0 the bulk specific entropy and $c_{p,J}$ the specific heat capacity, constant and associated with the reference state. Defining the capillary pressure as $p_c = p_i - p_w$ and

integrating (16) from the reference state, while using (17), we derive:

$$p_c = \left(\frac{\rho_i}{\rho_w} - 1\right) p_w + S_f\ (T_0 - T) + C_f\ \left(T - T_0 + T \ln \frac{T_0}{T}\right) \tag{18}$$

where $S_f = \rho_i \left(s_w^0 - s_i^0\right)$ is the entropy of fusion per unit of ice crystal volume, $C_f = \rho_i \left(c_{p,w} - c_{p,i}\right)$ the heat capacity difference between water and ice per unit of ice crystal volume. Term $\left(\frac{\rho_i}{\rho_w} - 1\right) p_w$ can be eventually neglected. Actually $S_f \simeq 1.2$ MPa and $C_f \simeq 2.1$ MPa from [Brun et al., 1977], so that we find $S_f \left(T_0 - T\right) \simeq 60$ MPa, $\left|C_f\ \left(T - T_0 + T \ln \frac{T_0}{T}\right)\right| \simeq 10$ MPa for a cooling equal to -50 ^{0}C. Since $\left|\frac{\rho_i}{\rho_w} - 1\right| \simeq 0.09$, a same order of magnitude for term $\left(\frac{\rho_i}{\rho_w} - 1\right) p_w$ requires the order of magnitude of liquid water pressure to be $p_w \equiv 10^4$ MPa. Such unrealistic values for the pore pressure would lead to the material failure, which is not observed here. Thus (18) is well approximated by

$$p_c = S_f\ (T_0 - T) + C_f\ \left(T - T_0 + T \ln \frac{T_0}{T}\right) = \mathrm{g}(T) \tag{19}$$

Function g(T) is the state function which relies the temperature T and the capillary pressure p_c once the thermodynamic equilibrium is reached between the liquid water and the ice already formed. In a first approximation, T_0 is evaluated by Raoult law as $T_0 = T_{00} - K\ m_0$, noting $T_{00} = 273.15$ K the bulk solidification temperature of pure water at atmospheric pressure, m_0 the initial molality (about 1 mol/kg for cement paste older than 90 days [Baron and Sauterey, 1982]) and K the cryoscopic Raoult coefficient, dependent on the solvent and irrespective to solute. In the case of water solvent, $K \simeq 1.86$ Kkg/mol [Zuber and Marchand, 2000].

Mechanical equilibrium of the ice/water interface (Young-Laplace law) gives:

$$p_c = \gamma\kappa \tag{20}$$

where $\gamma \simeq 36 + 0.25\ (T - T_{00})$ [Zuber and Marchand, 2004] is the water / ice interface energy and $\kappa = \frac{\mathrm{d}A_{wi}}{\mathrm{d}V_i} = \frac{1}{r_1} + \frac{1}{r_2}$ the interface curvature where A_{wi} is the water/ice interface area, V_i the ice crystal volume and $r_{i=1,2}$ are the principal curvature radii of the ice / water interface. We classically have:

$$\kappa = \frac{2}{r} \quad \text{for spherical ice crystal} \quad ; \quad \kappa = \frac{1}{r} \quad \text{for cylindrical ice crystal} \tag{21}$$

where r is the radius of the ice crystal which is related to the pore radius r_p and the unfreezable water layer length $e \simeq 9\mathring{A}$ by the relation [Brun et al., 1977, Dash et al., 1995]:

$$r = r_p - e. \tag{22}$$

From now, pores will be supposed to be cylindrical. Let use the common assumption that the ice crystal grows from a spherical interface and thaws from cylindrical one [Setzer, 1997]. The freezing and melting temperatures, respectively T_f and T_m, for an ice crystal just filling the cylindrical pore and in equilibrium with liquid water in adjacent pores, are related to the corresponding pore radius r_p from (19) to (22):

$$T_f = \mathrm{g}^{-1}\left(\frac{2\,\gamma}{r_p - e}\right) \quad \& \quad T_m^* = \mathrm{g}^{-1}\left(\frac{\gamma}{r_p - e}\right) \tag{23}$$

6.2 Determination of the pore radii distribution curve

Based on relation (23), the measurement of the successive freezing or melting temperatures provides the means of assessing the pore radii distribution of a porous material. However

it is well-known [Scherer, 1993, Béjaoui et al., 2002] that a liquid water filled pore of radius r_p does not generally freeze at the corresponding $T_f(r_p)$ in case of the commonly observed water supercooling (metastable liquid phase). Instead in-pore ice formation results from ice percolation through smaller (nanoscopic) channel-like pores connected to already frozen pores [Scherer, 1993] or from nucleation process which can only occur at a temperature lower than $T_f(r_p)$ [Corr, 2001]. On the other hand, on thawing, liquefaction appears necessarily at $T_m(r_p)$. This is attributed to the liquid layer, always present at the ice crystal surface, which acts as a nucleation scarf and thus prevents from metastability [Dash et al., 1995]. As a consequence, the thawing curve must be preferred to the freezing curve [Béjaoui et al., 2002], when aiming at establishing the pore radii distribution curve using thermoporometry concepts [Brun et al., 1977].

On thawing, (23) gives a relationship between temperature and assumed cylindrical pore radius. S_w is linked to the volume of frozen pores V_i by the relation $S_w = 1 - \frac{V_i}{Vpores} \Leftrightarrow V_i = V_{pores}(1 - S_w)$. Thus, $S_w - T_m$ thawing curves can be expressed as $V_i - r_p$ curves. The pore radius distribution curve φ is

$$\varphi(r_p) = \frac{\mathrm{d}V_i}{\mathrm{d}r_p}(r_p) \tag{24}$$

and is shown in figure 10 for P4-1d paste and in figure 11 for P5-1d. The pore radii range from 20 to 200 Å.

Pore radii distribution can also be obtained from sorption isotherm tests on 30 mg crushed samples placed into our home-made SD apparatus. The pore size curve is inferred from the sorption $S_w - p_c(rh)$ capillary curve through the BJH method which is

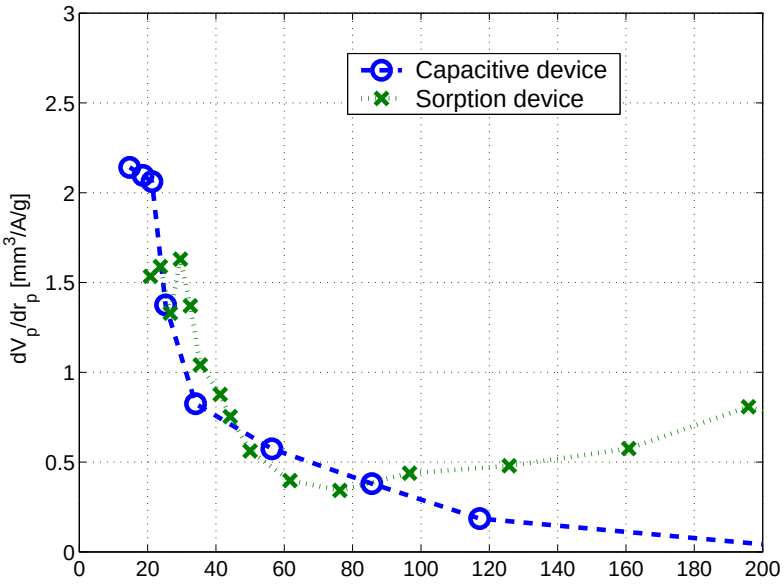

Figure 10: Comparison between pore radius distribution from thermoporometry using CS and from sorption isotherm using SD for $W/C = 0.4$ cement paste.

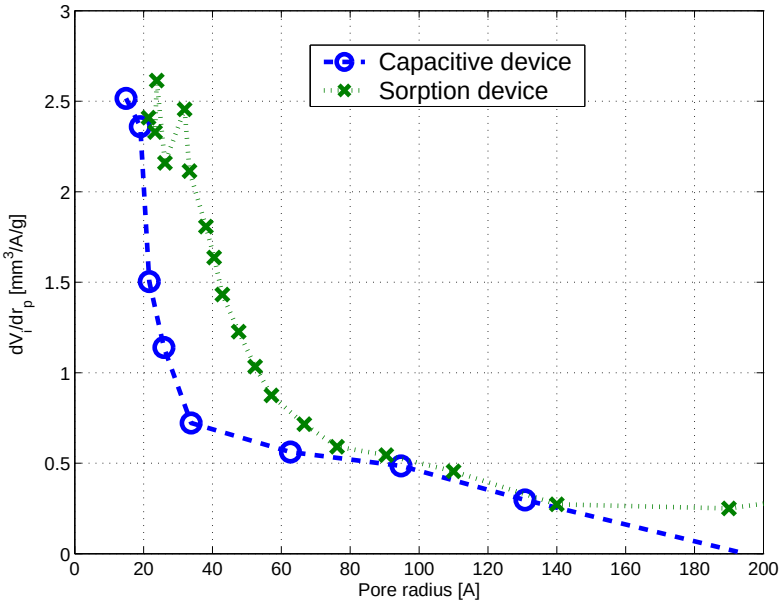

Figure 11: Comparison between pore radius distribution from thermoporometry using CS and from sorption isotherm using SD for $W/C = 0.5$ cement paste.

based on the thermodynamic and mechanical equilibrium between liquid water and water vapour [Barrett et al., 1951]. It gives a relation between capillary pressure, adsorbed layer length of capillary condensation water and pore diameter. Comparison of pore radii distributions obtained by SD or CS is shown in figures 10 and 11. All cement paste samples used in this study were of the same batch and conserved in the same condition (respectively P4-1d and P5-1d conditions). Slight differences at small pore radii may be explained by the fact that the temperature dependence of the thermodynamic coefficients was neglected. For the W/C=0.4 paste (figure 10) there is a peak in the distribution from sorption isotherm at about 200 Å. This peak is not present in the distribution obtained from the capacitive apparatus nor on the W/C=0.5 curves. This difference may be explained by the crushing operation on the specimens according to the SD procedure: the samples may have been internally microcracked contrary to the CS experimental procedure. In summary, it can be concluded that both methods yield pore size distributions in the same range of order.

6.3 Determination of freezable porous network surface area

6.3.1 Theoretical derivation

Mechanical equilibrium between liquid water and ice crystal may be written, using Laplace Law, as [Quinson et al., 1987]:

$$p_c = \gamma \frac{\mathrm{d}A_{wi}}{\mathrm{d}V_i} \tag{25}$$

Let $V_p = \phi V$ be the total volume of porous network, with V the porous medium volume. From the definition of the liquid water saturation ($S_w = V_w/V_p = 1 - V_i/V_p$) and under the assumption that the solid matrix is undeformable ($\mathrm{d}\phi = \mathrm{d}V = 0$), it is possible to express $\mathrm{d}V_i$ as:

$$\mathrm{d}V_i = -V_p \mathrm{d}S_w = -\phi V \mathrm{d}S_w \tag{26}$$

Finally, combining equations 25 and 26, Laplace law becomes:

$$\phi p_c = -\gamma\rho \frac{\mathrm{d}\omega_{wi}}{\mathrm{d}S_w} \tag{27}$$

where ρ is the apparent dry density of the porous medium and $\omega_{wi} = A_{wi}/\rho V$ the specific surface area of ice / liquid interface (surface area per unit of dried porous medium mass) during a thawing test. From the integration of (27), ω_{wi} can be evaluated as:

$$\omega_{wi} = \int_{S_w}^{1} \frac{\phi p_c}{\rho\gamma} \mathrm{d}S_w \tag{28}$$

Because of the existence of an unfreezable water layer between ice crystals and pore walls, ω_{wi} is not the frozen porous network specific surface (ω). In case of an elementary cylindrical pore with a radius $r_p = r_c + e$ (see figure 12), the relation between $\mathrm{d}\omega$ and $\mathrm{d}\omega_{wi}$ can be easily estimated by the relation:

$$\mathrm{d}\omega = \frac{r_c + e}{r_c} \mathrm{d}\omega_{wi} \tag{29}$$

Assuming the porous network to be composed by cylindrical pores, the explored specific surface area can be derived from (28) and (29):

$$\omega = \int_{S_w}^{1} \frac{r_c + e}{r_c} \frac{\phi p_c}{\rho\gamma} \mathrm{d}S_w \tag{30}$$

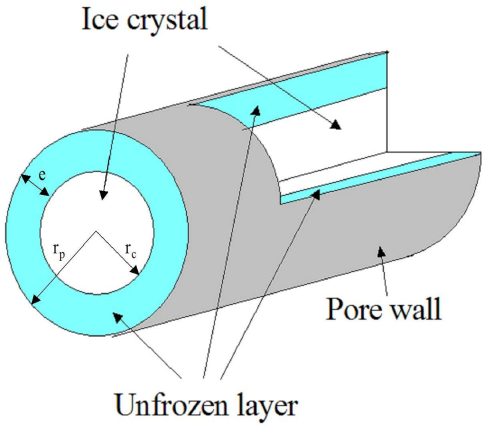

Figure 12: Schematic representation of an elementary cylindrical pore.

6.3.2 Application

Measurable specific surface area of the overall freezable porous network ($\mathcal{A}$ in m^2/g) will be the value of ω for $S_w \to S_{w,\min}$ where $S_{w,\min}$ is the volume ratio of unfreezable water. Thus, for cylindrical assumed pores, equation (30) leads to:

$$\mathcal{A} = \int_{S_{w,\min}}^{1} \frac{r_c + e}{r_c} \frac{\phi p_c}{\rho \gamma} \mathrm{d}S_w \tag{31}$$

Table 6 shows the $\mathcal{A}$-values obtained from the capacitive sensor (CS) based apparatus for P4-1d and P5-1d cement paste samples. It also contains the specific surface area values provided by MIP and sorption/desorption tests from specimens belonging to the same batch and curing conditions. Specific surface area values from MIP are based on the Rootare and Prenzlow equation [Rootare and Prenzlow, 1967]. Those from sorption/desorption isotherms rely on the BET theory analysis [Brunauer et al., 1938]. Numerical applica-

tions are made with $\rho = 1.67$ g/cm^3 for P4-1d, $\rho = 1.62$ g/cm^3 for P5-1d, and with values given in section 6.2.

Paste	MIP	**CS**	SD
P4-1d	13.31	**68.40**	118.50
P5-1d	16.81	**82.38**	145.46

Table 6: Comparison between specific surface area values from capacitive sensor (CS), mercury-injection porosimetry (MIP), and sorption/desorption (SD) techniques in m^2/g.

The CS values appear to be strongly higher than MIP ones. This large gap can be explained by the damage caused by the high pressure needed for the MIP experiment and the inability of the latter to scan finer porosity. Actually the mercury-injection porosimetry technique is known to underestimate the specific area [Raoof, 1998]. Furthermore, the lower values provided by the CS experiment by comparison to the SD experiment can be attributed to the screening effect of unfreezable water with regard to the roughness of the internal walls of the porous network. In addition, the CS cooling test is restricted to -45 ^{0}C whereas ice formation is still observed down to -80 ^{0}C [Jehng et al., 1996].

7 Conclusion

A spectroscopic-like dielectric capacitive apparatus was set-up in order to experimentally determine the thermodynamic state relation relying the ice content on the current tem-

perature. This quantitative method has been successfully applied to centimetric cement paste samples. The method exploits the high contrast existing in the radio frequency range between the dielectric properties of the liquid water and those of the other constituents. Actually, by combining the results provided by drying tests and freezing tests, theoretical and experimental considerations allow to derive the relation relying unambiguously the dielectric constant of a freezing porous material on both the liquid saturation and the temperature.

Two cement pastes with distinct water / cement ratio (W/C=0.4 and 0.5), cured in three different ways (moist, drying under $rh = 11\%$ at 20 ^{0}C, and oven-drying at 70 ^{0}C), have been tested. The experimental results agree well with the data existing in the literature obtained independently on the same kind of specimens by low temperature calorimetry. Pore radii distribution and specific surface area are found to be consistent with those obtained on similar samples from sorption/desorption isotherms by means of a home-made apparatus. Hence it can be concluded that the capacitive method here presented turns out to be one of the most appropriate to analyze the ice formation in cement-based materials, while in addition providing good insights into their pore structure.

Acknowledgements

We are grateful to J.P. Guilbaud for his contribution to the experimental set-up design, F. Martineau for sample fabrication, G. Foray-Thevenin and B. Crescini for providing cement pastes, P. Vié, V. Baroghel-Bouny and L. Routhe for mercury-injection porosime-

try measurements, S. Bichon for sorption/desorption measurements. The third author, Olivier Coussy, acknowledges the Miller Institute for Basic Research in Science, University of California Berkeley, for supporting his contribution to this work he completed as a Visiting Miller Research Professor during his sabbatical leave in the Fall 2004.

References

[Bager and Sellevold, 1986] Bager, D. and Sellevold, E. (1986). Ice formation in hardened cement paste - part II : Drying and resaturation on room temperature cured pastes. *Cement and Concrete Research*, 16:835–844.

[Baron and Sauterey, 1982] Baron, J. and Sauterey, R. (1982). *Le Béton Hydraulique - Connaissance et Pratique*. Presses de L'ENPC.

[Barrett et al., 1951] Barrett, E., Joyner, L., and Halenda, P. (1951). The determination of pore volume and area distributions in porous substances. i : Computations from nitrogen isotherms. *Journal of the American Chemical Society*, 73:373–380.

[Barthel et al., 1992] Barthel, J., Hetzenauer, H., and Buchner, R. (1992). Dielectric relaxation of aqueous electrolyte solutions. i- solvent relaxation of 1:2, 2:1 and 2:2 electrolyte solutions. *Berichte der Bunsen-Gesellschaft - Physical Chemistry Chemical Physics*, 96:988–997.

[Beaudoin and MacInnis, 1974] Beaudoin, J. and MacInnis, C. (1974). The mechanism of frost damage in hardened cement paste. *Cement and Concrete Research*, 4:139–147.

[Béjaoui et al., 2002] Béjaoui, S., Revertegat, E., and Bournazel, J.-P. (2002). Mécanismes de formation de la glace au sein des ptes de ciment et bétons. *Revue franaise de Génie Civil*, 6(7-8).

[Bitteli et al., 2004] Bitteli, M., Flury, M., and Roth, K. (2004). Use of dielectric spectroscopy to estimate ice content in frozen porous media. *Water resources research*, 40.

[Brun et al., 1977] Brun, M., Lallemand, A., Quinson, J., and Eyraud, C. (1977). A new method for the simultaneous determination of the size and the shape of pores : The thermopormetry. *Thermophysica Acta*, 21:59–88.

[Brunauer et al., 1938] Brunauer, S., Emmett, P., and Teller, E. (1938). Adsorption of gases in multimolecular layers. *Journal of American Chemical Society*, 60(2):309–319.

[Cole and Cole, 1941] Cole, K. and Cole, R. (1941). Dispersion and adsorption in dielectrics: I-alternating current characteristics. *Journal of Chemical Physics*, 9:341–351.

[Corr, 2001] Corr, D. (2001). *A microscopic study of ice formation and propagation in concrete*. PhD thesis, Berkeley, California, USA.

[Coussy, 2005] Coussy, O. (2005). Poromechanics of freezing materials. *Journal of the Mechanics and Physics of Solids - Submitted to publication*.

[Coussy and Fen-Chong, 2005] Coussy, O. and Fen-Chong, T. (2005). Crystallization, pore relaxation and cryosuction. *Comptes Rendus de mécanique*, page submitted to publication.

[Dash et al., 1995] Dash, J. G., Fu, H.-Y., and Wettlaufer, J. S. (1995). The premelting of ice and its environmental consequences. *Reports on Progress in Physics*, 58:115–167.

[Djaballah-Masmoundi, 1998] Djaballah-Masmoundi, N. (1998). *Modélisation et expérimentation de la perméabilité et des mécanismes de tranfert dans les milieux poreux au cours du gel*. PhD thesis, Université Pierre et Marie Curie, Paris VI, Paris, France.

[Ellison et al., 1996] Ellison, W., Lamkaouchi, K., and Moreau, J. (1996). Water: a dielectric reference. *Journal of Molecular Liquids*, 68:171–279.

[Fen-Chong et al., 2005] Fen-Chong, T., Fabbri, A., and Gaulard, F. (2005). Freezing and thawing porous media : Experimental study with a dielectric capacitive method. *C.R. Mecanique*, page Submitted to publication.

[Fen-Chong et al., 2004] Fen-Chong, T., Fabbri, A., Guilbaud, J.-P., and Coussy, O. (2004). Determination of liquid water content and dielectric constant in porous media by the capacitive method. *C.R. Mecanique*, 332:639–645.

[Gallé, 2001] Gallé, C. (2001). Effect of drying on cement based materials pore structure as identified by mercury intrusion porosimetry. *Cement and concrete Research*, 31.

[Jehng et al., 1996] Jehng, J., Sprague, D., and Halperin, W. (1996). Pore structure of hydrating cement paste by magnetic resonance relaxation analysing and freezing. *Magnetic Resonance Imaging*, 14(7/8):785–791.

[Kaatze, 1997] Kaatze, U. (1997). The dielectric properties of water in its different states of interaction. *Journal of Solution Chemistry*, 26(11):1049–1112.

[Kaufmann, 1999] Kaufmann, J. (1999). *Experimental identification of damage mechanisms in cementitious porous materials on phase transition of pore solution under frost deicing salt attack*. PhD thesis, École Polytechnique Fédérale de Lausanne, Ecublens, CH-1015 Lausanne.

[Kozlowski, 2003a] Kozlowski, T. (2003a). A comprehensive method of determining the soil unfrozen water curves. 1: Application of the term of convolution. *Cold Regions Science and Technology*, 36:71–79.

[Kozlowski, 2003b] Kozlowski, T. (2003b). A comprehensive method of determining the soil unfrozen water curves. 2: Stages of the phase change process in frozen soil-water system. *Cold Regions Science and Technology*, 36:81–92.

[Lindmark, 1997] Lindmark, S. (1997). *Mechanisms of salt frost scaling of portland cement-bound materials: studies and hypothesis*. PhD thesis, Lund Institute of Technology, Sweden.

[Mercury et al., 2001] Mercury, L., Vieillard, P., and Tardy, Y. (2001). Thermodynamics of ice polymorphs and ice-like water in hydrates and hydroxydes. *Applied Geochemistry*.

[Mironov et al., 2003] Mironov, V.-L., Kaupp, V.-H., Komarov, S.-A., and Kleshchenko, V.-N. (2003). Frozen soil dielectric model using unfrozen water spectroscopic parameters. In *International Geoscience and Remote Sensing Symposium (IGRASS)*, pages 4172–4174.

[Petrenko and Whitworth, 1999] Petrenko, V. F. and Whitworth, R. W. (1999). *Physics of Ice*. Oxford University Press.

[Pigeon, 1984] Pigeon, M. (1984). *Microstructure et résistance au gel des ciments et bétons*. PhD thesis, Université Pierre et Marie Curie, Paris 6, France.

[Quinson et al., 1987] Quinson, J. F., Astier, M., and Brun, M. (1987). Determination of surface areas by thermoporometry. *Applied Catalysis*, 30:123–130.

[Raoof, 1998] Raoof, A. (1998). *Adsorption distribution et dynamique de l'eau dans les milieux poreux*. Laboratoire Central des Ponts et Chausses, Paris.

[Raoof and Guilbaud, 1995] Raoof, A. and Guilbaud, J. P. (1995). An automatic micro-gravimetric water sorption apparatus. In *Proceedings of the International Workshop on Mass-Energy Transfert and Deterioration of Building Components - Model and Characterisation of Transfert Properties*.

[Rootare and Prenzlow, 1967] Rootare, H. and Prenzlow, C. (1967). Surface areas from mercury porosimeter measurements. *Journal of Physical Chemistry*, 71(8):2733–2736.

[Scherer, 1993] Scherer, G. W. (1993). Freezing gels. *Journal of Non Crystalline Solids*, 155:1–25.

[Sellevold and Bager, 1980] Sellevold, E. J. and Bager, D. H. (1980). Low temperature calorimetry as a pore structure probe. 7^{TH} *International Congress on the Chemistry of Cement, Paris*, 4:394–399.

[Setzer, 1997] Setzer, M. J. (1997). Action of frost and deicing chemicals: Basic phenomena and testing. In Marchand, J., Pigeon, M., and Setzer, M. J., editors, *RILEM Proceedings 30, Freeze-Thaw Durability of Concrete*. E & FN SPON.

[Spaans and Baker, 1995] Spaans, E. J. A. and Baker, J. M. (1995). Examining the use of TDR for measuring liquid water content in frozen soils. *Water Resources Research*, 31:2917–2925.

[Thimus et al., 1991] Thimus, J. F., Aguirre-Puente, J., and Cohen-Tenoudji, F. (1991). Determination of unfrozen water content of an overconsolidated clay down to -160^{o}C by sonic approaches - comparison with classical methods. In Yu and Wang, editors, *Ground Freezing 91*, pages 83–88. Balkema, Rotterdam.

[Tran and Dupas, 1988] Tran, N. L. and Dupas, A. (1988). Méthodes diélectriques de mesure de la teneur en eau dans les matériaux de génie civil. In Raimbault, G., editor, *Journées de Physique, Les Arcs, 14 - 17 déc. 1987*, volume 2 (L'eau dans les matériaux) of *Bulletin de Liaison des Laboratoires des Ponts & Chaussées*, pages 157–164.

[Wang et al., 1996] Wang, K., Monteiro, P. J. M., Rubinsky, B., and Arav, A. (1996). Microscopic study of ice propagation in concrete. *ACI Materials Journal*, pages 370–377.

[Watanabe and Mizogucchi, 2002] Watanabe, K. and Mizogucchi, M. (2002). Amount of unfrozen water in frozen porous media saturated with solution. *Cold Regions Science and Technology*, 34:103–110.

[Zakri et al., 1998] Zakri, T., Laurent, J.-P., and Vauclin, M. (1998). Theoretical evidence for lichtenecker's mixture formulae based on the effective medium theory. *Journal of Physics D: Applied Physics*, 31:1589–1594.

[Zhang et al., 2003] Zhang, L., Shi, J., Zhang, Z., and Zhao, K. (2003). The estimation of dielectric constant of frozen soil-water mixture at microwave bands. In *International Geoscience and Remote Sensing Symposium (IGRASS)*, pages 2903–2905.

[Zuber and Marchand, 2000] Zuber, B. and Marchand, J. (2000). Modeling the deterioration of hydrated cement systems exposed to frost action - part 1 : description of the mathematical model. *Cement and Concrete Research*, 30.

[Zuber and Marchand, 2004] Zuber, B. and Marchand, J. (2004). Predicting the volume instability of hydrated cement systems upon freezing using poro-mechanics and local phase equilibra. *Concrete Science Engineering*, 37(268):257–270.